SCIENCE CHINA Materials ARTICLES

mater.scichina.com link.springer.com

Published online 15 October 2018 | https://doi.org/10.1007/s40843-018-9352-7

Sci China Mater 2019, 62(4): 527–535

Ultralight 3D-γ-MnOOH porous materials fabricated by hydrothermal treatment and freeze-drying

Yanqiu Wang, Lu Chen, Min Chen, Zhaoxiang Zhong*, Qingwei Meng and Weihong Xing*

ABSTRACT **Creating three-dimensional (3D) ultralight metal oxide using cost-effective precursors and facile approaches is important. Here, shape-controlled γ-MnOOH (density lower than 0.078 g cm^{-3}) with a continuously 3D porous network (3D-γ-MnOOH) was successfully fabricated with $KMnO_4$, $MnCl_2$ and NaOH *via* hydrothermal treatment and freeze-drying. The hydrothermal condition and the amount of reactants were systematically investigated, and the optimal procedure occurs at 180°C for 10 h with the molar ratios of $NaOH/KMnO_4$ and $MnCl_2/KMnO_4$ as 5.0 and 3.5, respectively. Owing to the low density, 3D network, and the filling of air inside the channel, the new γ-MnOOH can float on the water for at least 4 months with complete structure. The formation and floating mechanism of the 3D-γ-MnOOH were also explored. This new 3D-γ-MnOOH could be utilized in oil absorption.**

Keywords: low-density, 3D-γ-MnOOH, porous material, freeze-drying

INTRODUCTION

Ultralight three-dimensional (3D) materials have been attracting tremendous interest, and a number of low-density 3D materials have been synthesized by carbon aerogels [1], metallic foams [2], graphene aerogels [3,4], and carbon nanotube-graphene hybrid aerogels [5]. These materials possess a continuously cross-linked network, low thermal conductivity, high porosity and high surface area, which broadens their applications in oil or heavy metal adsorption [6,7], catalysis [8], thermal insulating materials [9], gas storage [10] and supercapacitors [11]. Nyström *et al.* [12] prepared ultralight 3D hybrid gold amyloid aerogel *via* a sol-gel approach for wet and continuous flow catalysis. Chen *et al.* [13] fabricated low-density 3D magnetic foams by calcining a composite sponge at 400°C. This material exhibited good oil-water separation performance. Tang *et al.* [14] synthesized 3D copper nanowire aerogels using a facile freeze-casting method, which combined the good mechanical and electrical properties of metals with the low density of an aerogel. However, in most cases, these low-density 3D materials were synthesized by complex technologies or using expensive materials. Therefore, it is important to find cost-effective materials to prepare low-density 3D materials for large-scale production and industrial applications.

Manganese oxides are abundant, affordable, and environmentally friendly, and can be used in catalysis [15–17], adsorption [18,19], electrochemistry [20] and energy storage, such as lithium batteries [21,22] and supercapacitors [23,24]. Meanwhile, manganese oxide can also be used as precursors for the synthesis of spinel-type lithium manganese oxides [25,26] and several other phases of manganese oxides [27–29]. Therefore, many researchers have considerable interest in preparing manganese oxide with specific structures and morphologies by controllable synthesis routes. Manganese oxide currently possesses various shapes: nanoparticles [30,31], nanorods [32,33], nanowires [29], nanosheets [34], nanobelts [20], nanotubes [35], and nanoflowers [36]. However, only a few low-density 3D-structure manganese oxides have been reported. Jung *et al.* [37] reported a 3D $K_{2-x}Mn_8O_{16}$ aerogel prepared *via* direct hydrothermal method with remarkable density, surface area and porosity. Rong *et al.* [38] reported a pure 3D MnO_2 framework by directly freezing a mixture of MnO_2 nanosheets and nanorods, which exhibited good removal performance for HCHO. 3D MnO_2 exhibits high adsorption of organic solutions, which indicates that appropriate method is important to prepare low density manganese oxides to absorb spilled oil on the water.

Here, we prepared ultralight 3D-γ-MnOOH by simple

State Key Laboratory of Materials-Oriented Chemical Engineering, National Engineering Research Center for Special Separation Membrane, Nanjing Tech University, Nanjing 210009, China

* Corresponding authors (emails: zhongzx@njtech.edu.cn (Zhong Z); Xingwh@njtech.edu.cn (Xing W))

hydrothermal treatment and freeze-drying process. Hydrothermal route is a relatively facile procedure under mild environments. Moreover, hydrothermal products have high crystallinity and controllable crystal size. It is easy to adjust the shape of the 3D-γ-MnOOH by changing the shape of the hydrothermal reaction vessels. Meanwhile, the unique porous 3D structure enables the low-density γ-MnOOH to float on water for at least 4 months without changes. Furthermore, the chemical composition, morphology, synthesis mechanism, and floating mechanism of the 3D-γ-MnOOH are studied in detail. The low-density 3D structure and floating properties of 3D-γ-MnOOH endow the potential application in oil absorption, catalysis, and flexible electrodes.

EXPERIMENTAL SECTION

Materials

All of the chemicals used for the fabrication of 3D-γ-MnOOH were of analytical grade and used as received. Potassium permanganate ($KMnO_4$) was purchased from Shanghai Lingfeng Chemical Reagent Co., Ltd. (Shanghai, China). Manganese(II) chloride tetrahydrate ($MnCl_2{\cdot}4H_2O$) and sodium hydroxide (NaOH) were obtained from Xilong Scientific Co., Ltd. (Shantou, China). Deionized water was used throughout the experiments.

Preparation of precursor of 3D-γ-MnOOH

$MnCl_2$ solution (25 mL, 0.5 mol L^{-1}) was slowly introduced to a mixture of 0.59 g $KMnO_4$, 0.75 g NaOH and 30 mL deionized water with constant agitation at room temperature, and the precursor of 3D-γ-MnOOH was obtained as a well-dispersed brownish suspension solution. After collecting the precipitate by filtration, amorphous manganese oxides were obtained *via* freeze-drying, while γ-MnOOH nanoparticles were obtained *via* drying in a 60°C oven.

Preparation of 3D-γ-MnOOH

First, the as-prepared manganese oxide suspension solution was poured into a Teflon-lined stainless-steel autoclave, sealed, and then placed in a 180°C air-dry oven for 10 h. Then the reactor was naturally cooled to room temperature, and the brownish precipitates with ideal shapes were collected, and dried in a lyophilizer for 48 h to obtain the low-density 3D-γ-MnOOH. The optimal condition was investigated to get 3D-γ-MnOOH with good structure and high crystallinity, including adjusting the amount of NaOH and $MnCl_2$, as well as the hydrothermal time.

Characterization

The chemical composition and crystallographic information of the fabricated materials were obtained by a power X-ray diffractometer (XRD, MiniFlex300/600, Rigaku, Japan). The surface structure and morphologies of the materials were investigated with a scanning electron microscope (SEM, Hitachi S4800, Japan) and transmission electron microscope (TEM, TF20, Joel 2100F, Japan). The average fiber diameter and diameter distribution were measured by IPP6.0 image analysis software. N_2 adsorption-desorption data were measured using a specific surface analyzer (BET, Micromeritics ASAP 2460, USA). The specific surface area of the 3D-γ-MnOOH was obtained from the N_2 adsorption data in the relative pressure range from 0.05 to 0.3 by using the Brunauer-Emmett-Teller (BET) method. The as-prepared material was also characterized with Fourier transform infrared spectrometer (FTIR, Nicolet 8700, USA). The surface electronic structure of the light materials was performed using X-ray photoelectron spectroscopy (XPS, Escalab 250XI, Thermo Scientific, USA).

RESULTS AND DISCUSSION

Morphological and structural analysis

The typical low-density 3D γ-MnOOH was fabricated *via* hydrothermal reaction and freeze-drying. The overall fabrication procedure is illustrated in detail in Fig. 1. First, amorphous manganese oxide suspensions were synthesized by slowly dropping $MnCl_2$ into a mixed solution of NaOH and $KMnO_4$ at room temperature. The amorphous manganese oxides first dissolved and then recrystallized into γ-MnOOH nanoparticles under hydrothermal conditions. Afterwards, the adjacent γ-MnOOH nanoparticles orientated themselves to attach or self-assemble along the specific direction to form brown cross-linked nanorod precipitates. The 3D-γ-MnOOH was prepared *via* freeze drying of the brownish precipitates. To the best of our knowledge, this is the first report of a facile method for high-purity, low-density 3D γ-MnOOH, without the assistance of any template agent or surfactant. The shape of the 3D-γ-MnOOH can be easily modified by changing the shape of the hydrothermal reaction vessels. Heart-shaped and cylindrical 3D-γ-MnOOH materials could be synthesized *via* the shape of the reaction vessels (Fig. 2a, b). The as-prepared 3D-γ-MnOOH has a remarkably low density down to 0.078 g cm^{-3} as calculated by the ratio of its mass and volume (i.e., 1.401 g in 17.85 cm^3, Fig. 2b, c). This makes the 3D-γ-MnOOH 52 to 54 times lighter than the tradi-

Figure 1 Schematic of the preparation of 3D-γ-MnOOH *via* hydrothermal reaction and freeze-drying.

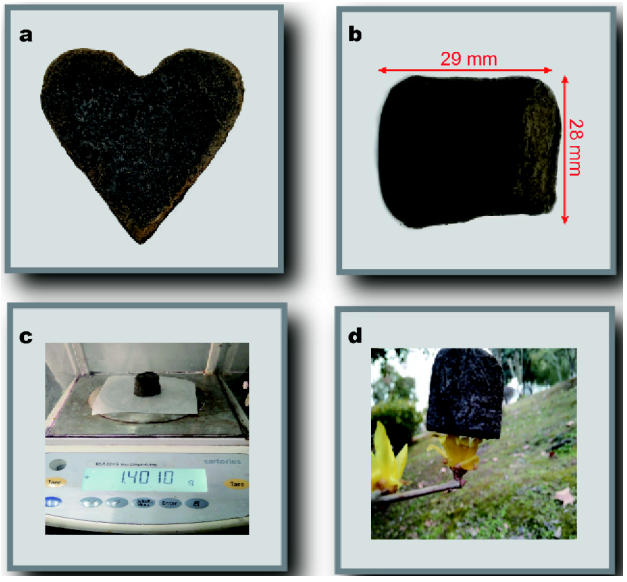

Figure 2 (a) Heart-shaped and cylindrical 3D-γ-MnOOH. (b, c) Weight measurement of 3D-γ-MnOOH, with an estimated density of 0.078 g cm^3 (i.e., 1.401 g in 17.85 cm^3); and (d) digital photo of a cylindrical 3D-γ-MnOOH standing on a Wintersweet flower.

tional γ-MnOOH at equivalent volume, confirming the successful synthesis of a low-density material. Similar to some low-density aerogels [14,39], the 3D-γ-MnOOH with volume of 17.85 cm^3 can even stand on a Wintersweet flower without deformation (Fig. 2d).

The structure and morphologies of the low-density 3D-γ-MnOOH and its precursors were characterized by SEM. As shown in Fig. 3a, e, the freeze-dried precursors exhibit irregular features, including nanoparticles, nanorods, and nanosheets. Fig. 3b, f show that the dried precursors are composed of homogeneous nanoparticles. The 3D-γ-MnOOH is composed of nanorods (with a length longer than 5 μm) that randomly intertwine and form many mesopores resulting in a 3D network (Fig. 3c, g). The inset of Fig. 3g shows the nanorod diameter ranging from 30 to 150 nm with the average nanorod diameter 50 nm. Fig. 3d shows the TEM image of the 3D-γ-MnOOH nanorod. As shown in Fig. 3h, the nanorod shows well-resolved lattice fringes with an adjacent interplanar spacing of ~0.34 nm, which can be assigned to the (11−1) facets of γ-MnOOH. In addition, the SEM and TEM images also show that the nanorods have a high aspect ratio with a representative length longer than 5 μm and diameters less than 50 nm. This feature is conducive to the fabrication of low-density 3D γ-MnOOH. Meanwhile, the specific surface area of 3D-γ-MnOOH is 10 m^2 g^{-1}.

XRD patterns of freeze-dried precursors, dried precursors, and 3D-γ-MnOOH are shown in Fig. 4a–c. Except for the peaks of the MnOOH (2θ=19.20°, JCPDS Card No. 18-0804), the obtained freeze-dried precursors also contain MnO_2 (2θ=31.59° and 33.28°, JCPDS Card No. 12-0141) and MnO (2θ=34.91° and 40.55°, JCPDS Card No. 07-0230). The dried precursor also shows a main peak that matches the (002) plane of MnOOH (2θ=19.20°, JCPDS Card No. 18-0804) (Fig. 4b). Based on the SEM and TEM images and the XRD patterns, the amorphous MnO_2 and MnO dissolve and subsequently condense and recrystallize to form a (002) plane of γ-MnOOH under hydrothermal conditions. Fig. 4c shows that the XRD pattern of 3D-γ-MnOOH matches the single monoclinic phase of γ-MnOOH, with lattice parameters a=5.300 Å, b=5.278 Å, and c=5.307 Å and space group $P21/c$. The diffraction peaks at 2θ=26.15°, 33.94°, 35.54°, 37.17°, 39.65°, 41.07°, 51.22°, 53.78°, 54.94°, 55.55°, 61.60°, and 64.83° correspond to the (11−1), (020), (111), (002), (12−1), (012), (022), (22−2), (31−1), (031), (131), and (202) phase of γ-MnOOH, respectively (JCPDS Card No. 41-1379). The diffraction peaks also suggest that the 3D-γ-MnOOH has high

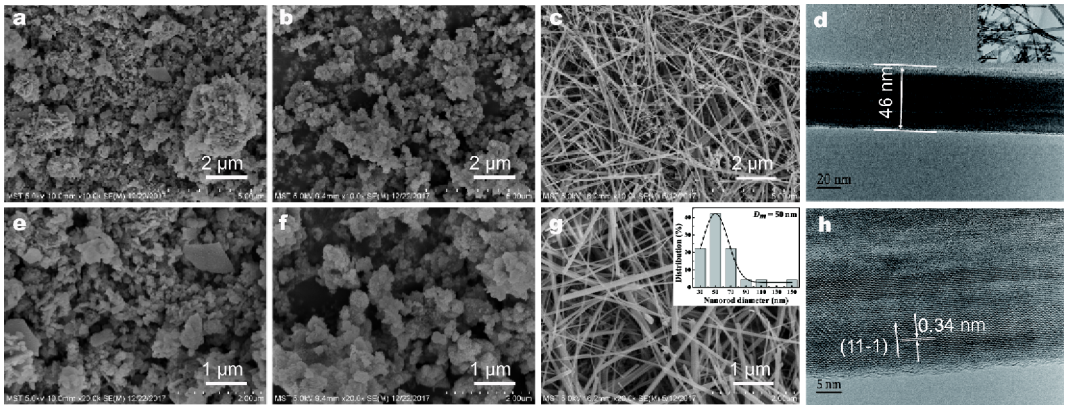

Figure 3 SEM images of freeze-dried precursors (a, e), dried precursors (b, f), and 3D-γ-MnOOH (c, g), and the diameter distribution diagram of 3D-γ-MnOOH nanorods (inset of g); TEM images of 3D-γ-MnOOH nanorod (d, h).

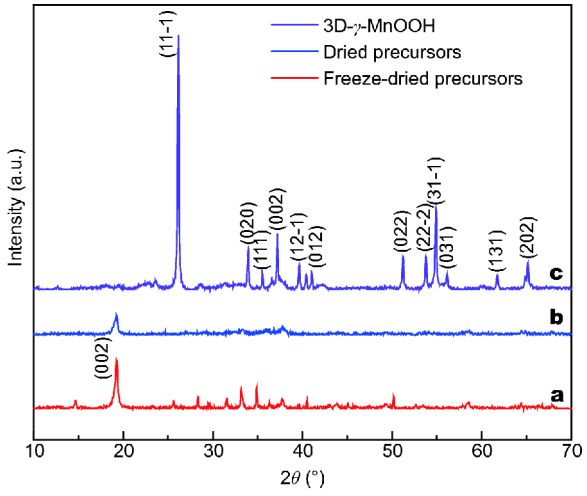

Figure 4 XRD patterns of freeze-dried precursors (a), dried precursors (b), and 3D-γ-MnOOH (c).

crystallinity.

As shown in Fig. 5a, FTIR spectrum of the 3D-γ-MnOOH shows the absorption bands at 447, 490, 592, and 644 cm^{-1} derived from the vibration of Mn—O. Moreover, the three peaks at 1,080, 1,120, and 1,150 cm^{-1} are representative of the bending mode γ-OH, δ-2-OH and δ-1-OH, respectively [39]. As expected, the FTIR spectrum shows a broad band between 2,600 and 2,700 cm^{-1} that results from the O—H stretching related to the hydrogen bonding with an O—H···O length of approximately 2.60 Å in the structure of manganite [40,41]. The absorption band located near 2,080 cm^{-1} is ascribed to 2,670 cm^{-1} (the –OH stretching band) minus 592 cm^{-1} (the excited lattice). This FTIR spectrum resembles that of manganite [20,40].

The surface chemical compositions of the products were further studied by XPS (Fig. 5b). All of the measurements were performed with reference to the binding energy (BE) of C (1s) (284.5 eV) as an internal standard. The signals of manganese, oxygen, and carbon were recorded as the Auger peaks of Mn(LMM) and O(KLL). The existence of the C (1s) photoelectron peak can also be observed, because the carbon dioxide in the air is trapped on the surface of the materials. Fig. 5c, d exhibit the XPS spectra of Mn (2p) and O (1s) peaks. Fig. 5c shows that the Mn (2p) was deconvoluted into Mn ($2p_{3/2}$) and Mn ($2p_{1/2}$) peaks at approximately 642.4 and 654.1 eV, respectively, in agreement with the characteristics of γ-MnOOH [42,43]. The multiplet splitting energy of Mn (3s) in the product is 5.2 eV, while the smaller Mn (3s) splitting energies for tetravalent and bivalent Mn were 4.6 and 5.8 eV [44,45], respectively. The splitting energy of Mn(3s) increased with decreasing Mn oxidation state, and the manganese oxidation state of the synthetic materials corresponds to trivalent manganese. In addition, the O (1s) spectrum of the materials in Fig. 5d is parsed into three functional groups, corresponding to O^{2-}, OH^-, and O (1s), which are consistent with oxygen types in ideal γ-MnOOH. The O^{2-} only bonds to Mn^{3+} and OH^- directly bonds to hydrogen. Meanwhile, O (1s) receives equal contributions from O^{2-}, OH^-, as well as H_2O (water is from the physical and chemical adsorption of the obtained materials). In this work, we assign the deconvoluted peaks at 529.9, 531.1, and 532.5 eV to O^{2-}, OH^- and H_2O species, respectively. The characterization is very close to the results reported by Gao and Banerjee *et al.* [42,43].

Floatation performance

Fig. 6a, b show that the heart-shaped and cylindrical 3D-

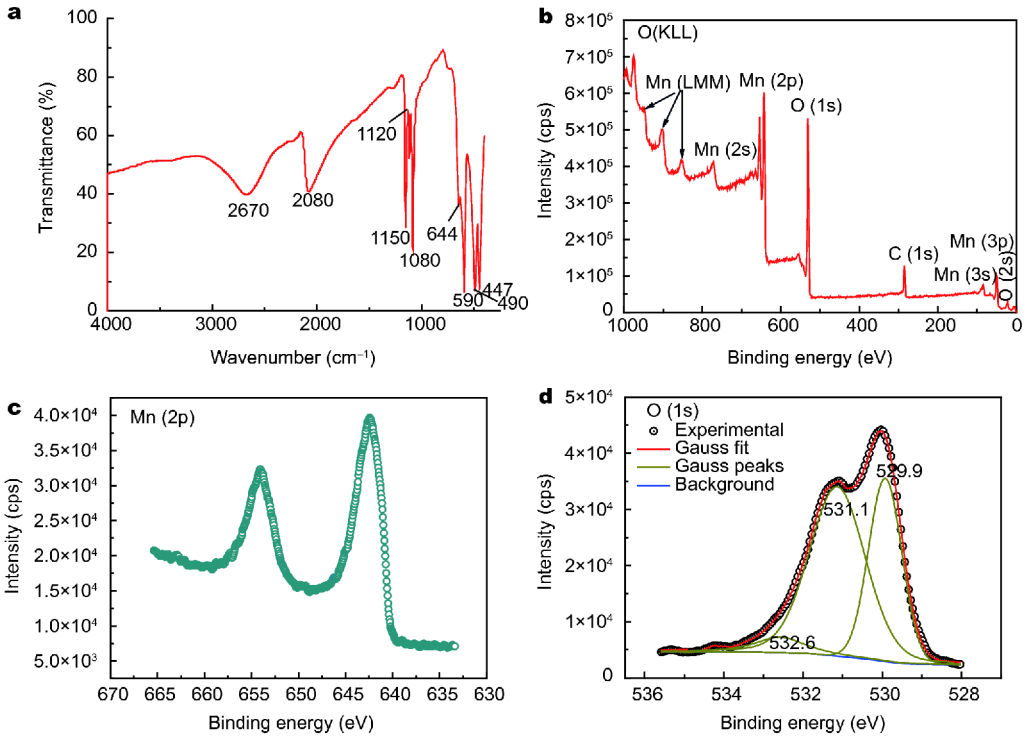

Figure 5 (a) FTIR spectrum of 3D-γ-MnOOH; XPS spectrum of 3D-γ-MnOOH (b); XPS spectra of the Mn (2p) (c) and O (1s) (d).

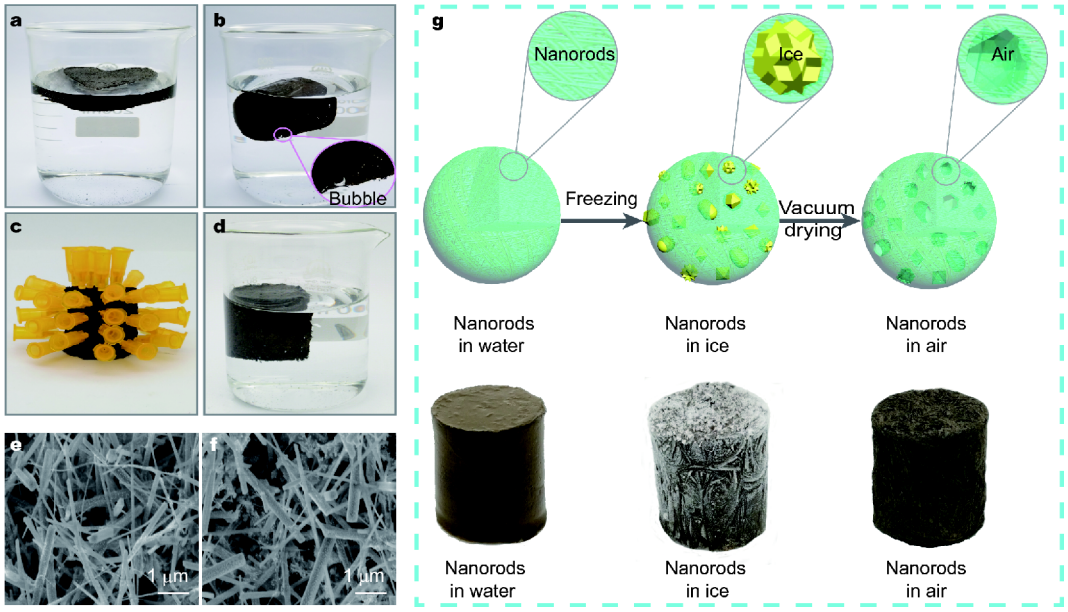

Figure 6 Digital photos of (a) heart-shaped and (b) cylindrical 3D-γ-MnOOH floating on the water; (c) more than 100 syringe needle holes were created on the surface of 3D-γ-MnOOH; (d) 3D-γ-MnOOH with 100 holes that can still float on water; SEM image of (e) as-prepared 3D-γ-MnOOH and (f) submerged 3D-γ-MnOOH; and (g) schematic of the formation process of the floatable porous 3D-γ-MnOOH.

γ-MnOOH can float on water. This feature is due to the low-density 3D structure of 3D-γ-MnOOH, and the trapped air in the channels of 3D-γ-MnOOH. When 3D-γ-MnOOH is placed in water, there are many small bubbles entrapped on the interface of 3D-γ-MnOOH (inset of Fig. 6b). Accordingly, we see that the inner

channel of 3D-γ-MnOOH is filled with air, and water slowly drives the bubbles out. 3D-γ-MnOOH was still able to float on the water even after more than 100 holes were made in the 3D-γ-MnOOH with needles (Fig. 6c, d). This confirms that 3D-γ-MnOOH has a very stable porous spatial structure. The formation mechanism of floatable porous 3D-γ-MnOOH filled with air is shown in Fig. 6g. The precipitate with cross-linked nanorods surrounded by water can offer phase separation during freezing. That is, the low temperature changes the water into ice, and water is separated from the nanorods. Ice crystals are sublimated during the vacuum drying process. After ice crystals sublimate, holes are formed in the material, resulting in a continuous porous 3D network structure, and air enters the channels. The 3D-γ-MnOOH can still float on water for at least 4 months until the air in the channels is completely driven away by water. After 3D-γ-MnOOH sank under the water, it was removed and dried. The re-dried 3D-γ-MnOOH could then float on water again. In contrast to the original 3D-γ-MnOOH (Fig. 6e), the porous network of the submerged 3D-γ-MnOOH (Fig. 6f) was not destroyed reconfirming the good mechanical stability of 3D-γ-MnOOH.

Oil absorption performance

3D-γ-MnOOH has good potential for absorbing oil because of its uniform macroporous structure and excellent oleophilicity (Fig. S1). The capacity for oil absorption can be referred to as the oil absorption rate ($g\ g^{-1}\ s^{-1}$), which is defined as the quantity of absorbed oil per gram of dry 3D-γ-MnOOH per second. The series of photographs in Fig. 7a illustrate that when a small piece of 3D-γ-MnOOH was placed on oil (1,330 mg, strained with oil blue N dye), the oil was immediately absorbed by 3D-γ-MnOOH and completely disappeared within 5 s. The average oil absorption rate of 3D-γ-MnOOH can reach ~1.52 $g\ g^{-1}\ s^{-1}$, which is nearly 3 times higher than that of previously reported graphene aerogels (~0.57 $g\ g^{-1}\ s^{-1}$) [46]. This clearly indicates the great potential of using 3D-γ-MnOOH to remove oil spills and leaks. In addition, the oil can be quickly ignited and burnt off after being absorbed by 3D-γ-MnOOH (Fig. 7b). After combustion, 3D-γ-MnOOH still maintains its original shape, size, and 3D network structure, except for a color change from brownish black to yellowish brown. This indicates that it has good stability under combustion. 3D-γ-MnOOH has excellent oleophilicity and floatability. The 3D network structure of 3D-γ-MnOOH may help to remove the heat generated from combustion. When 3D-γ-MnOOH was contacted with 10 drops of oils floating

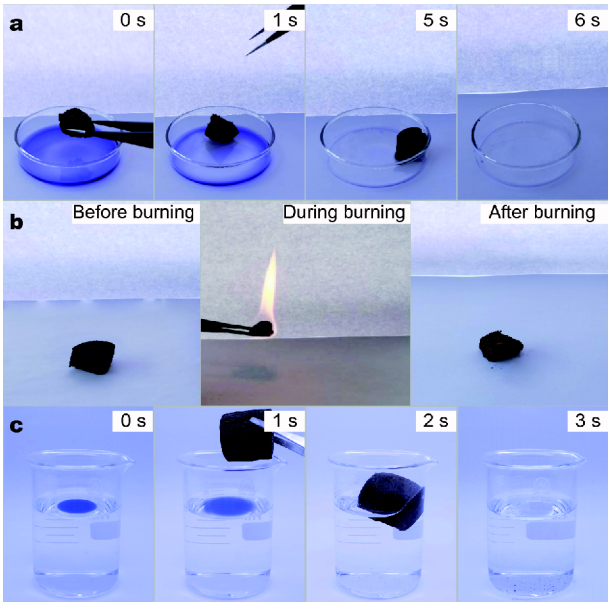

Figure 7 (a) Absorption process of oils (strained with oil blue N dye) of 3D-γ-MnOOH within 5 s. (b) Photos showing the process of recycling 3D-γ-MnOOH *via* combustion. (c) 3D-γ-MnOOH removes the oils on water surface.

on the surface of water, it absorbed the oils completely and rapidly and remained floating on the water. There is basically no oil residue when 3D-γ-MnOOH is removed from the water (Fig. 7c). Accordingly, 3D-γ-MnOOH also shows great potential for removing oil from the water surface.

Optimum synthesis procedures

XRD and SEM were used to investigate the crystallographic information and morphologies of hydrothermal products while considering the influence of NaOH on the fabrication process of 3D-γ-MnOOH. When the mole ratio of NaOH/$KMnO_4$ is between 4.0 and 6.0, the diffraction peaks correspond to the characteristic single phase of γ-MnOOH (Fig. S2c–e). However, when the ratio of NaOH/$KMnO_4$ is outside the range of 4.0 and 6.0, the products consist of a variety of manganese oxides, including γ-MnOOH (2θ=37.28°), MnO_2 (2θ=19.76°), and $Mn(OH)_4$ (2θ=37.60°) (see Fig. S2a, b and f). Meanwhile, when the NaOH/$KMnO_4$ ratio is 5.0, the crystallinity of the γ-MnOOH is the highest. SEM images in Fig. S3 show the structures and morphologies of products fabricated using different ratio of NaOH/$KMnO_4$. When the NaOH/$KMnO_4$ ratio is 5.0, these uniform nanorods are cross-linked to form a continuous network. The SEM images show that the hydrothermal products are consistent with the XRD analysis, namely that the

optimal ratio of $NaOH/KMnO_4$ is 5.0.

The effect of the amount of $MnCl_2$ on the composition and morphologies of hydrothermal products was considered while keeping the ratio of $NaOH/KMnO_4$ at 5.0 and the hydrothermal temperature at 180°C. The XRD data (see Fig. S4) show that when the ratio of $MnCl_2/KMnO_4$ was up to 2.5, similar XRD patterns were detected, and the peaks correspond to γ-MnOOH. The crystallinity of the γ-MnOOH is the best, when the ratio of $MnCl_2/KMnO_4$ is 3.5. The morphologies of the as-prepared materials were further studied in Fig. S5. Nevertheless, only Fig. S5d appears to have pure and relatively uniform nanorods that are cross-linked to form a 3D network. The others have nanoparticles attached to the surface of the nanorods. The SEM results nicely match the XRD measurements, confirming that the optimal ratio of $MnCl_2/KMnO_4$ is 3.5.

The effect of hydrothermal time on the synthesis process of 3D-γ-MnOOH was considered. The reactions were carried out with hydrothermal times ranging from 0 to 5.5 h. The diffraction peaks in Fig. S6a exhibit main peaks (0 h) that match the (002) plane of MnOOH. After 0.5 h, almost all of the diffraction peaks match a monoclinic phase of γ-MnOOH (Fig. S6c–e). Moreover, the growth of γ-MnOOH transformed from (002) to (11−1), and the crystallinity of γ-MnOOH was constantly increasing. In addition, an extra peak appears in Fig. S6c and d that matches potassium chloride (KCl) (2θ=28.31°, JCPDS Card No. 04-0587). This peak disappears as the hydrothermal treatment time extends to 5.5 h, indicating KCl contributes to the formation of 3D-γ-MnOOH. SEM images were further analyzed for morphologies of the products. Fig. 8a shows that only uniform particles were observed in the products (0 h). The nanoparticles self-assemble along a specific direction, and the number of nanoparticles continues to decrease with longer hydrothermal times and they disappear completely when the hydrothermal time approaches 5.5 h (Fig. 8b–d). The number, diameter, and length of the nanorods increase with hydrothermal time and eventually form a continuous 3D network. The XRD and SEM results show that the γ-MnOOH nanoparticles self-assemble along a [11−1] direction to form cross-linked γ-MnOOH nanorods.

CONCLUSIONS

In conclusion, low-density 3D-γ-MnOOH with porous 3D network and well-defined shape was successfully fabricated *via* the hydrothermal reaction of $KMnO_4$, $MnCl_2$ and NaOH. 3D-γ-MnOOH can float on water for at least 4 months. The ratio of $NaOH/KMnO_4$ and $MnCl_2/KMnO_4$, as well as the hydrothermal time on the hydrothermal crystallization of products were optimized. Cross-linking γ-MnOOH nanorods follows a dissolution–recrystallization mechanism, i.e., amorphous MnO_2 and MnO dissolve and recrystallize onto a (002) plane of γ-MnOOH nanoparticles. Subsequently, the adjacent MnOOH nanoparticles will self-assemble along the [11−1] direction; thereafter, the gaps between the nanoparticles will disappear and eventually fuse together to form nanorods. After that, the air will drive away the condensed water inside the precipitates to produce low-density 3D-γ-MnOOH during the freeze-drying step. The novel ultralight 3D-γ-MnOOH has significant potential applications in oil absorption.

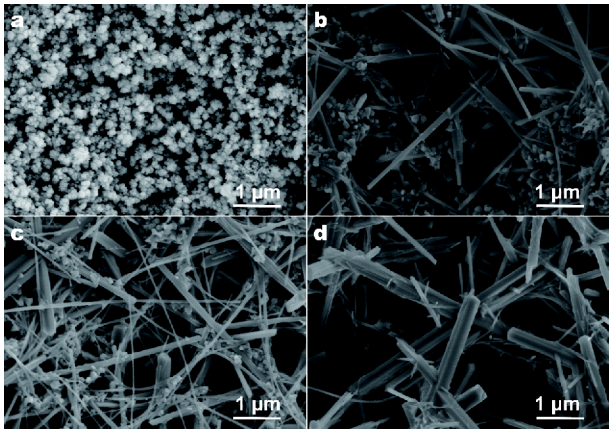

Figure 8 SEM images of the obtained products for different hydrothermal treatment times: (a) 0, (b) 0.5, (c) 1 and (d) 5.5 h.

Received 8 June 2018; accepted 7 September 2018; published online 15 October 2018

1 Yang Y, Tong Z, Ngai T, *et al.* Nitrogen-rich and fire-resistant carbon aerogels for the removal of oil contaminants from water. ACS Appl Mater Interfaces, 2014, 6: 6351–6360
2 Tappan BC, Huynh MH, Hiskey MA, *et al.* Ultralow-density nanostructured metal foams: combustion synthesis, morphology, and composition. J Am Chem Soc, 2006, 128: 6589–6594
3 Yue C, Feng J, Feng J, *et al.* Ultralow-density and high-strength graphene aerogels composites for thermal insulation. Mater Lett, 2017, 188: 169–171
4 Hu H, Zhao Z, Wan W, *et al.* Ultralight and highly compressible graphene aerogels. Adv Mater, 2013, 25: 2219–2223
5 Hu H, Zhao Z, Gogotsi Y, *et al.* Compressible carbon nanotube–graphene hybrid aerogels with superhydrophobicity and superoleophilicity for oil sorption. Environ Sci Technol Lett, 2014, 1: 214–220
6 Korhonen JT, Kettunen M, Ras RHA, *et al.* Hydrophobic nanocellulose aerogels as floating, sustainable, reusable, and recyclable oil absorbents. ACS Appl Mater Interfaces, 2011, 3: 1813–1816
7 Yun L, Zhao J, Kang X, *et al.* Preparation and properties of monolithic and hydrophobic gelatin–silica composite aerogels for

oil absorption. J Sol-Gel Sci Technol, 2017, 83: 197–206
8 Feng JJ, Lin XX, Chen LX, *et al.* Ionic liquid-assisted synthesis of composition-tunable cross-linked AgPt aerogels with enhanced electrocatalysis. J Colloid Interface Sci, 2017, 498: 22–30
9 Yoldas BE, Annen MJ, Bostaph J. Chemical engineering of aerogel morphology formed under nonsupercritical conditions for thermal insulation. Chem Mater, 2000, 12: 2475–2484
10 Weng Q, Wang X, Zhi C, *et al.* Boron nitride porous microbelts for hydrogen storage. ACS Nano, 2013, 7: 1558–1565
11 Xu Y, Sheng K, Li C, *et al.* Self-assembled graphene hydrogel *via* a one-step hydrothermal process. ACS Nano, 2010, 4: 4324–4330
12 Nyström G, Fernández-Ronco MP, Bolisetty S, *et al.* Amyloid templated gold aerogels. Adv Mater, 2016, 28: 472–478
13 Chen N, Pan Q. Versatile fabrication of ultralight magnetic foams and application for oil–water separation. ACS Nano, 2013, 7: 6875–6883
14 Tang Y, Yeo KL, Chen Y, *et al.* Ultralow-density copper nanowire aerogel monoliths with tunable mechanical and electrical properties. J Mater Chem A, 2013, 1: 6723
15 Smith PF, Deibert BJ, Kaushik S, *et al.* Coordination geometry and oxidation state requirements of corner-sharing MnO_6 octahedra for water oxidation catalysis: an investigation of manganite (γ-MnOOH). ACS Catal, 2016, 6: 2089–2099
16 Sun W, Hsu A, Chen R. Carbon-supported tetragonal MnOOH catalysts for oxygen reduction reaction in alkaline media. J Power Sources, 2011, 196: 627–635
17 Shang C, Yang M, Wang Z, *et al.* Encapsulated MnO in N-doping carbon nanofibers as efficient ORR electrocatalysts. Sci China Mater, 2017, 60: 937–946
18 Bochatay L, Persson P. Metal ion coordination at the water–manganite (γ-MnOOH) interface. J Colloid Interface Sci, 2000, 229: 593–599
19 Pan G, Qin Y, Li X, *et al.* EXAFS studies on adsorption–desorption reversibility at manganese oxides–water interfaces. J Colloid Interface Sci, 2004, 271: 28–34
20 Bayoudh A, Etteyeb N, Kossai R. Hydrothermal synthesis, characterization and electrochemical properties of γ-MnOOH nanobelts. Ceramics Int, 2015, 41: 12273–12279
21 Zhan D, Yang F, Zhang Q, *et al.* Effect of solid-state reaction temperature on electrochemical performance of $LiMn_2O_4$ submicro-rods as cathode material for Li-ion battery by using γ-MnOOH submicro-rods as self-template. Electrochim Acta, 2014, 129: 364–372
22 He L, Zhang S, Wei X, *et al.* Synthesis and electrochemical performance of spinel-type $LiMn_2O_4$ using γ-MnOOH rods as self-template for lithium ion battery. J Power Sources, 2012, 220: 228–235
23 Liu Z, Xing Y, Fang S, *et al.* Facile synthesis of γ-MnOOH nanotubes and their application in electrochemical capacitors. J Mater Sci-Mater Electron, 2015, 26: 5975–5979
24 Zheng M, Xiao X, Li L, *et al.* Hierarchically nanostructured transition metal oxides for supercapacitors. Sci China Mater, 2018, 61: 185–209
25 Bai Z, Fan N, Sun C, *et al.* Facile synthesis of loaf-like $ZnMn_2O_4$ nanorods and their excellent performance in Li-ion batteries. Nanoscale, 2013, 5: 2442–2447
26 Xia Y, Yoshio M. Studies on Li-Mn-O spinel system (obtained from melt-impregnation method) as a cathode for 4 V lithium batteries Part II. Optimum spinel from g-MnOOH. J Power Sources, 1995, 57: 125–131
27 Folch B, Larionova J, Guari Y, *et al.* Synthesis of MnOOH nanorods by cluster growth route from $[Mn_{12}O_{12}(RCOO)_{16}(H_2O)_n]$ (R=CH_3, C_2H_5). Rational conversion of MnOOH into Mn_3O_4 or MnO_2 nanorods. J Solid State Chem, 2005, 178: 2368–2375
28 Wei C, Xu C, Li B, *et al.* Formation and conversion mechanisms between single-crystal gamma-MnOOH and manganese oxides. Mater Res Bull, 2012, 47: 1740–1746
29 Zhang YC, Qiao T, Hu XY, *et al.* Simple hydrothermal preparation of γ-MnOOH nanowires and their low-temperature thermal conversion to β-MnO_2 nanowires. J Cryst Growth, 2005, 280: 652–657
30 Zhao D, Yang X, Zhang H, *et al.* Effect of environmental conditions on Pb(II) adsorption on β-MnO_2. Chem Eng J, 2010, 164: 49–55
31 Li C, Han X, Cheng F, *et al.* Phase and composition controllable synthesis of cobalt manganese spinel nanoparticles towards efficient oxygen electrocatalysis. Nat Commun, 2015, 6: 7345
32 Hosono E, Ichihara M, Zhou H. Fabrication of MnOOH nanorods on a substrate in an oxygen bubbled solution with superhydrophobic properties. Nanotechnology, 2008, 19: 395606
33 Chen ZW, Lai JKL, Shek CH. Nucleation site and mechanism leading to growth of bulk-quantity Mn_3O_4 nanorods. Appl Phys Lett, 2005, 86: 181911
34 Cheng JH, Shao G, Yu HJ, *et al.* Excellent catalytic and electrochemical properties of the mesoporous MnO_2 nanospheres/nanosheets. J Alloys Compd, 2010, 505: 163–167
35 Zheng D, Sun S, Fan W, *et al.* One-step preparation of single-crystalline β-MnO_2 nanotubes. J Phys Chem B, 2005, 109: 16439–16443
36 Yan D, Zhang H, Li S, *et al.* Formation of ultrafine three-dimensional hierarchical birnessite-type MnO_2 nanoflowers for supercapacitor. J Alloys Compd, 2014, 607: 245–250
37 Jung SM, Jung HY, Fang W, *et al.* A facile methodology for the production of in situ inorganic nanowire hydrogels/aerogels. Nano Lett, 2014, 14: 1810–1817
38 Rong S, Zhang P, Yang Y, *et al.* MnO_2 framework for instantaneous mineralization of carcinogenic airborne formaldehyde at room temperature. ACS Catal, 2017, 7: 1057–1067
39 Sun S, Wang S, Xia T, *et al.* Hydrothermal synthesis of a MnOOH/three-dimensional reduced graphene oxide composite and its electrochemical properties for supercapacitors. J Mater Chem A, 2015, 3: 20944–20951
40 Kohler T, Armbruster T, Libowitzky E. Hydrogen bonding and Jahn–Teller distortion in groutite, α-MnOOH, and manganite, γ-MnOOH, and their relations to the manganese dioxides ramsdellite and pyrolusite. J Solid State Chem, 1997, 133: 486–500
41 Sharma PK, Whittingham MS. The role of tetraethyl ammonium hydroxide on the phase determination and electrical properties of γ-MnOOH synthesized by hydrothermal. Mater Lett, 2001, 48: 319–323
42 Gao T, Krumeich F, Nesper R, *et al.* Microstructures, surface properties, and topotactic transitions of manganite nanorods. Inorg Chem, 2009, 48: 6242–6250
43 Nesbitt HW, Banerjee D. Interpretation of XPS Mn(2p) spectra of Mn oxyhydroxides and constraints on the mechanism of MnO_2 precipitation. Am Miner, 1998, 83: 305–315
44 Oku M, Hirokrwa K, Rkeda S. X-ray photoelectron spectroscopy of manganese-oxygen systems. J Electron Spectrosc & Relat Phenom, 1975, 7: 465
45 Ardizzone S, Bianchi CL, Tirelli D. Mn_3O_4 and γ-MnOOH powders, preparation, phase composition and XPS characterisation.

Colloids Surfs A-Physicochem Eng Aspects, 1998, 134: 305–312
46 Bi H, Xie X, Yin K, *et al.* Spongy graphene as a highly efficient and recyclable sorbent for oils and organic solvents. Adv Funct Mater, 2012, 22: 4421–4425

Acknowledgements This work was supported by the National Natural Science Foundation of China (U1510202), the National Key R&D Program (2016YFC0204000), and Jiangsu Province Scientific Supporting Project (BK20170046).

Author contributions Xing W and Zhong Z conceived and designed the experiments; Wang Y, Chen L, Chen M, Meng Q carried out the experiments. Wang Y and Zhong Z wrote this paper. All authors contributed to the general discussion.

Conflict of interest The authors declare no conflict of interest.

Supplementary information Supporting data are available in the online version of the paper, including the XRD patterns and TEM images of the synthetic materials *via* using different amounts of lithium hydroxide and manganese chloride, as well as the XRD patterns of the synthetic materials *via* different hydrothermal times.

Yanqiu Wang is currently pursuing her master degree under the supervision of Prof. Weihong Xing at the College of Chemical Engineering in Nanjing Tech University. Her research interest is novel structural metal oxides and their application.

Zhaoxiang Zhong is a professor at the State Key Laboratory of Materials-Oriented Chemical Engineering in Nanjing Tech University. He received his PhD from Nanjing Tech University, Nanjing (China) in 2007. He is currently the young editor of *Journal of China Chemical Engineering* and the executive director of China Environmental Science Society. He also hosts the National Key R&D Project and Jiangsu Outstanding Youth Fund Project. His research interest includes air purification membrane materials and environmental functional nanomaterials.

Weihong Xing is the vice-president of Nanjing Tech University. She received her BSc degree (1991), MSc degree (1994) and PhD degree (2002) in chemical engineering from Nanjing Tech University. She is currently the Deputy Director of the National Membrane Separation Technology Standardization Committee, Vice Chairman of China Membrane Industry Association, and Director of the National Engineering Research Center for Special Separation Membrane. Her main research interest focuses on the research and application of membrane materials.

水热合成和冷冻干燥相结合制备超轻三维多孔γ-MnOOH材料

汪艳秋, 陈璐, 陈敏, 仲兆祥*, 孟庆伟, 邢卫红*

摘要 超轻三维多孔金属氧化物材料在许多应用中起着重要作用, 因此采用低成本的材料和简便的方法制备它们显得非常重要. 本文以高锰酸钾、氯化锰和氢氧化钠为原料, 结合水热合成法和冷冻干燥法首次制备出超低密度(<0.078 g cm^{-3})、形状可控和连续多孔的三维氢氧化氧锰(3D-γ-MnOOH). 系统地研究了反应物添加量和水热反应时间对3D-γ-MnOOH合成过程的影响, 得出制备3D-γ-MnOOH 的最优工艺条件: NaOH/$KMnO_4$和$MnCl_2$/$KMnO_4$的摩尔比分别为5.0和3.5, 水热温度和时间分别为180°C和10 h. 由于γ-MnOOH具有低密度和充满空气的三维孔道结构, 使其可以在水中漂浮4个月以上, 并保持微结构不变. 分析探讨了3D-γ-MnOOH的微结构形成机制和漂浮机理. 超轻3D-γ-MnOOH的成功制备将促进其在吸油、储能、催化剂载体等领域的应用.

